Characterization of the degradation mechanisms of lysine–derived aliphatic poly(ester urethane) scaffolds

ARTICLE *in* BIOMATERIALS · JANUARY 2011

Impact Factor: 8.56 · DOI: 10.1016/j.biomaterials.2010.08.108 · Source: PubMed

7 AUTHORS, INCLUDING:

Andrea E Hafeman
Vanderbilt University
16 PUBLICATIONS **323** CITATIONS
SEE PROFILE

Hak-Joon Sung
Vanderbilt University
68 PUBLICATIONS **1,145** CITATIONS
SEE PROFILE

Lillian B Nanney
Vanderbilt University
174 PUBLICATIONS **7,332** CITATIONS
SEE PROFILE

Scott A Guelcher
Vanderbilt University
108 PUBLICATIONS **1,918** CITATIONS
SEE PROFILE

Biomaterials 32 (2011) 419–429

Contents lists available at ScienceDirect

Biomaterials

journal homepage: www.elsevier.com/locate/biomaterials

Characterization of the degradation mechanisms of lysine-derived aliphatic poly (ester urethane) scaffolds

Andrea E. Hafeman [a,b], Katarzyna J. Zienkiewicz [a,b], Angela L. Zachman [c], Hak-Joon Sung [c], Lillian B. Nanney [d], Jeffrey M. Davidson [e,f], Scott A. Guelcher [a,b,*]

[a] Department of Chemical & Biological Engineering, Vanderbilt University, Nashville, USA
[b] Center for Bone Biology, Vanderbilt University, 2301 Vanderbilt Place, PMB 351604, Nashville, TN 37235-1604, USA
[c] Department of Biomedical Engineering, Vanderbilt University, Nashville, TN, USA
[d] Department of Plastic Surgery, Vanderbilt University Medical Center, Nashville, TN, USA
[e] Department of Pathology, Vanderbilt University Medical Center, Nashville, TN, USA
[f] Research Service, VA Tennessee Valley Healthcare System Nashville, TN, USA

ARTICLE INFO

Article history:
Received 6 August 2010
Accepted 30 August 2010
Available online 22 September 2010

Keywords:
Polyurethane
Biodegradation
Macrophage
Oxidation
Hydrolysis
Scaffold

ABSTRACT

Characterization of the degradation mechanism of polymeric scaffolds and delivery systems for regenerative medicine is essential to assess their clinical applicability. Key performance criteria include induction of a minimal, transient inflammatory response and controlled degradation to soluble non-cytotoxic breakdown products that are cleared from the body by physiological processes. Scaffolds fabricated from biodegradable poly(ester urethane)s (PEURs) undergo controlled degradation to non-cytotoxic breakdown products and support the ingrowth of new tissue in preclinical models of tissue regeneration. While previous studies have shown that PEUR scaffolds prepared from lysine-derived polyisocyanates degrade faster under *in vivo* compared to *in vitro* conditions, the degradation mechanism is not well understood. In this study, we have shown that PEUR scaffolds prepared from lysine triisocyanate (LTI) or a trimer of hexamethylene diisocyanate (HDIt) undergo hydrolytic, esterolytic, and oxidative degradation. Hydrolysis of ester bonds to yield α-hydroxy acids is the dominant mechanism in buffer, and esterolytic media modestly increase the degradation rate. While HDIt scaffolds show a modest (<20%) increase in degradation rate in oxidative medium, LTI scaffolds degrade six times faster in oxidative medium. Furthermore, the *in vitro* rate of degradation of LTI scaffolds in oxidative medium approximates the *in vivo* rate in rat excisional wounds, and histological sections show macrophages expressing myeloperoxidase at the material surface. While recent preclinical studies have underscored the potential of injectable PEUR scaffolds and delivery systems for tissue regeneration, this promising class of biomaterials has a limited regulatory history. Elucidation of the macrophage-mediated oxidative mechanism by which LTI scaffolds degrade *in vivo* provides key insights into the ultimate fate of these materials when injected into the body.

1. Introduction

A variety of synthetic polymers have been investigated as biodegradable scaffolds and delivery systems for regenerative medicine, such as poly(lactic-*co*-glycolic acid) (PLGA) [1], polyanhydrides (PAA) [2], tyrosine-derived polycarbonates [3], polyphosphazenes [4], and poly(propylene fumarate)s (PPF).[5] Characterization of the degradation mechanism is essential to assess the clinical applicability of biomaterials. Key performance criteria include induction of a minimal, transient inflammatory response and controlled degradation to soluble non-cytotoxic breakdown products that are cleared from the body by physiological processes (e.g., the Krebs cycle). [6]

Biodegradable poly(ester urethane)s (PEURs), which were first investigated as scaffolds for tissue regeneration 20 years ago[7,8], have good biocompatibility and favorable mechanical properties. Scaffolds fabricated from PEUR networks and segmented elastomers undergo controlled degradation to non-cytotoxic breakdown products [9–15] and support the ingrowth of new tissue in preclinical models of both soft [16–18] and hard [19–21] tissue regeneration. PEURs, which are synthesized from the condensation

* Corresponding author. Center for Bone Biology, Vanderbilt University, 2301 Vanderbilt Place, PMB 351604, Nashville, TN 37235-1604, USA. Tel.: +1 615 322 9097; fax: +1 615 343 7951.
E-mail address: scott.guelcher@vanderbilt.edu (S.A. Guelcher).

0142-9612/$ – see front matter © 2010 Elsevier Ltd. All rights reserved.
doi:10.1016/j.biomaterials.2010.08.108

reaction of an isocyanate-functional polyisocyanate (or prepolymer) and a polyester polyol, incorporate three types of degradable linkages: ester bonds in the polyester backbone, urethane bonds resulting from the reaction of the polyisocyanate with a polyol, and urea bonds resulting from the reaction of the polyisocyanate with a polyamine or water. While polyesters are known to hydrolyze to α-hydroxy acids, there is a lack of consensus on the stability of the urethane and urea bonds under physiological conditions. For polymers synthesized from lysine-derived polyisocyanates, some studies have reported hydrolysis of urethane linkages to yield lysine [12,13], while others have reported that urethane and urea linkages are only enzymatically degraded [11,22].

Previous studies have reported that biostable polyurethanes, which typically incorporate polyether or polycarbonate polyols, undergo enzymatic hydrolysis and oxidative degradation mediated by the interaction of inflammatory cells with the material [23–27]. Neutrophils and monocyte-derived macrophages cultured on biostable poly(carbonate-) and poly(ether-) urethanes secrete cholesterol esterase, carboxyl esterase, and serine proteases, which are the most active enzymes mediating hydrolytic degradation of these polymers [26]. In particular, secretion of cholesterol esterase increases as monocytes that are recruited to the implantation site differentiate into macrophages [28]. Biostable polyurethanes also undergo oxidative degradation mediated by macrophage-secreted reactive oxygen species (ROS). ATR-FTIR spectra of explanted poly(ether-) and poly(carbonate-) urethanes demonstrate evidence of oxidative chain scission and crosslinking over time [29,30].

Biodegradable PEUR elastomers incorporating a chain extender that is recognizable by an enzyme have been reported to show enzymatic degradation of the hard segment [11,31]. However, the effects of enzymatic and oxidative reactions on the degradation rate of PEURs not incorporating recognizable sites have not been investigated extensively. Recent observations that lysine-derived PEUR networks undergo faster degradation under *in vivo* compared to *in vitro* conditions [12,32] suggest that these materials undergo cell-mediated degradation. In this study, we investigated the role of esterolytic enzymes and reactive oxygen species secreted by macrophages on the degradation of aliphatic and lysine-derived PEUR networks under both *in vitro* and *in vivo* conditions.

2. Materials and methods

2.1. Materials

Glycolide and D,L-lactide were obtained from Polysciences (Warrington, PA), triethylene diamine (TEDA) catalyst was received from Goldschmidt (TEGOAMIN33, Hopewell, VA), polyethylene glycol (PEG, 600 g mol^{-1}) was supplied by Alfa Aesar (Ward Hill, MA), and glycerol was obtained from Acros Organics (Morris Plains, NJ). Lysine triisocyanate (LTI) was purchased from Kyowa Hakko USA (New York), and hexamethylene diisocyanate trimer (HDIt, Desmodur N3300A) was received as a gift from Bayer Material Science, LLC (Pittsburgh, PA). Monobasic sodium phosphate buffer, sodium azide, hydrogen peroxide, and cobalt chloride were purchased from Fisher Scientific (Pittsburgh, PA), while all other reagents were purchased from Sigma–Aldrich (St. Louis, MO). Glycerol and PEG were dried at 10 mm Hg for 3 h at 80 °C, and ε-caprolactone was dried over anhydrous magnesium sulfate. All other materials were used as received [33].

2.2. PEUR scaffold synthesis

The polyol component of the PEUR scaffolds comprised a polyester triol (900 g mol^{-1}) synthesized by reacting the glycerol starter, cyclic ester monomers (ε-caprolactone, glycolide, and D,L-lactide), and stannous octoate catalyst under dry argon for 36 h at 140 °C [15,32,34]. The resulting polyester triol was vacuum-dried at 80 °C for 14 h. Two triols with different half-lives ($t_{1/2}$) were synthesized to evaluate the effects of hydrolytic degradation: (a) 6C, with a backbone comprising 60% caprolactone, 30% glycolide, and 10% lactide ($t_{1/2}$ = 20 days); and (b) 7C, with a backbone comprising 70% caprolactone, 20% glycolide, and 10% lactide ($t_{1/2}$ = 225 days) [34].

Scaffolds were synthesized by reactive liquid molding of: (a) a polyisocyanate comprising either hexamethylene diisocyanate trimer (HDIt) or lysine triisocyanate (LTI), and (b) a hardener component comprising the polyester triol, 1.5 parts per hundred parts polyol (pphp) water, 4.5 pphp (1.5 pphp for LTI foams) TEGOAMIN33 catalyst, 1.5 pphp sulfated castor oil stabilizer, and 4.0 pphp calcium stearate pore opener [32]. The polyisocyanate was added to the hardener and mixed for 15 s in a Hauschild DAC 150 FVZ-K SpeedMixer™ (FlackTek, Inc., Landrum, SC). The targeted index (the ratio of NCO to OH equivalents times 100) was 115. To examine the effects of a hydrophilic polyether on the degradation rate, some materials were synthesized with poly(ethylene glycol) (PEG, 600 g mol^{-1}), such that the total polyol component consisted of 50 mol-% PEG and 50 mol-% polyester triol.

2.3. In vitro degradation of PEUR scaffolds

Long-term scaffold degradation rates were evaluated by measuring the mass loss for up to 36 weeks. Triplicate 10-mg samples were incubated in 1 ml phosphate buffered saline (PBS) on a shaker at 37 °C [32]. At each time point, scaffolds were removed from the buffer, rinsed in deionized water, dried under vacuum for 48 h, and weighed. The medium was not changed until the targeted time point to minimize phase separation errors resulting from disintegration of the scaffold at longer time points. The degradation media were used for the HPLC analysis of the breakdown products (Section 2.5). At 4, 8, and 12 weeks, core densities were determined from mass and volume measurements of cylindrical foam cores (7 mm × 10 mm) [32]. The core porosities (ε_C) were subsequently calculated from the measured density values [32]. The scaffold morphology was assessed by scanning electron microscopy (Hitachi S-4200 SEM, Finchampstead, UK).

Degradation of PEUR scaffolds is significantly faster under *in vivo* compared to *in vitro* conditions, suggesting that enzymatic or oxidative reactions mediate degradation *in vivo* [6,26,32]. To investigate the effects of esterolytic and oxidative conditions on scaffold degradation, materials were incubated in the presence of each of the following: cholesterol esterase, carboxyl esterase, lipase, hydrogen peroxide (H_2O_2), and buffer alone (control). Short-term *in vitro* degradation rates were evaluated under constant-sink conditions by replacing the medium every 3–4 days (which was necessary to maintain enzyme activity) and measuring the mass loss for 10 weeks. Triplicate 25-mg samples were incubated in 1 ml of the buffer control (0.5 M monobasic sodium phosphate buffer with 0.2% w/w sodium azide), esterolytic, or oxidative media at 37 °C. The enzyme concentrations, determined from previous literature as well as by the solubility limits of the enzymes in the media, were as follows: 1 U/mL cholesterol esterase (CE), 1 U/mL carboxyl esterase (CXE), and 10 U/mL lipase (L) [35]. The oxidative medium comprised 20 wt% hydrogen peroxide (H_2O_2) in 0.1 M cobalt chloride (Cl_2Co) [36]. The cobalt ion and hydrogen peroxide react to form hydroxyl radicals, simulating the oxidative radicals present at the material–macrophage interface. The medium was changed every 3–4 days to maintain enzyme activity, which was verified with a nonspecific activity assay based on the enzymatic conversion of *p*-nitrophenyl butyrate into *p*-nitrophenyl [27,37].

2.4. Dynamic mechanical properties

Dynamic mechanical properties of the scaffolds were measured using dynamic mechanical analysis (DMA) in compression and tension modes after 4, 8, and 12 weeks' degradation time. Cylindrical 7 × 6 mm samples were compressed along the axis of foam rise. The relaxation modulus was evaluated as a function of time with stress relaxation under 2% strain and 0.2-N static force. Stress–strain curves were generated by controlled-force compression of the cylindrical foam cores at 37 °C. With an initial force of 0.1 N, each sample was deformed at 0.1 N/min until it reached 50% strain (i.e. 50% of its initial height). The Young's modulus was determined from the slope of the initial linear region of each stress–strain curve [38]. Due to their elasticity, the scaffolds could not be compressed to failure, so the compressive stress was measured 1 min after the application of 50% strain using the DMA in stress relaxation mode [39]. Tensile testing was performed on thin, rectangular scaffold samples (10 mm long × 5 mm wide × 1.7 mm thick). Stress–strain curves were generated by stretching the samples (1% strain/minute) until failure. The Young's modulus was calculated as described above, and the tensile strength was reported as the stress (kPa) at failure.

2.5. Analysis of scaffold degradation products

Lactic (from D,L-lactide), glycolic (from glycolide), 6-hydroxycaproic (from ε-caprolactone), and cyanuric (from HDIt) acids were separated by isocratic elution in a Transgenomic ion exchange column (ICSep ICE-ION-300 Column 7.8 × 300 mm). The degradation products were passed through a guard column at 80 °C using 0.001 N sulfuric acid as eluent and analyzed by a UV detector at 210 nm. With a flow rate of 0.5 mL/min, the standard peaks for cyanuric, glycolic, lactic, and 6-hydroxycaproic acid eluted at 14.3, 15.4, 16.1, and 30.2 min, respectively. Samples were analyzed by an external standard curve in the range from 2.5 μg/mL to 100 μg/mL of each acid using the Waters Breeze system.

Lysine and ethanoloamine in the breakdown products were derivatized with 5-(Dimethylamino)naphthalene-1-sulfonyl chloride (dansyl chloride, DNS–Cl) and quantified by HPLC. 50 μL of each sample was added to 225 μL dansyl chloride (40 mM in acetonitrile) and 225 μL borate buffer (pH 9.5). The mixtures were vortexed for 10 s and incubated at 55 °C for 30 min. After cooling to room temperature,

Table 1
HPLC gradient program with two mobile phases at a 1 mL/min flow rate: (A) 0.1% (v/v) trifluoroacetic acid in water, and (B) 90% (v/v) acetonitrile with 0.1% trifluoroacetic acid.

Time (min)	% B
0–2	20
2–6	20 → 29
6–7	29 → 42
7–12	42 → 43
12–13	43 → 95
13–15	95
15–17	95 → 20
17–20	20

samples were syringe-filtered (0.2 μm) and injected into the column. The separation was performed using an HPLC system equipped with a Waters 1525 binary pump, an XTerra guard column (RP C8 5 μm 3.9 × 20 mm), an Xterra reverse-phase column (C18 5 μm 4.6 × 250 mm), and a 2487 UV–vis detector (230 nm).Samples were eluted using the gradient program listed in Table 1 with two mobile phases at a 1 mL/min total flow rate: (A) 0.1% (v/v) trifluoroacetic acid in water, and (B) 90% (v/v) acetonitrile with 0.1% trifluoroacetic acid. The lysine–DNS–Cl and ethanolamine–DNS–Cl peaks eluted at approximately 5.5 and 6.1 min, respectively. The concentrations of lysine and ethanolamine in each sample were calculated from an external standard curve ranging from 0.1 μg/mL to 5 μg/mL.

2.6. In vitro culture of macrophages on PEUR scaffolds

6C/LTI scaffolds were cut into thin 20 × 1-mm discs, sterilized by gamma irradiation, and placed in 24-well plates. RAW 264.7 murine macrophages (5×10^4 cells/well) were cultured with the materials in α-MEM with 10% FBS [40]. Each well contained 1 mL culture medium, which was replaced every 3 days. At two weeks, the media were removed and the scaffolds with seeded cells were fixed in 4% glutaraldehyde for 2 h followed by osmium tetroxide for another 2 h. The materials were then vacuum-dried before observation with SEM.

Intracellular ROS levels and secretion of nitric oxide (NO) and tumor necrosis factor (TNF)-α to culture media were measured from Raw 264.7 cells grown on 6C/LTI and 6C/HDIt scaffolds for 7 days ($n = 4$). The control comprised tissue culture polystyrene. Intracellular H_2O_2 levels were determined through incubation with an H_2O_2-sensitive fluorophore dichlorofluorescein diacetate (DCFDA, Molecular Probes) [41,42]. Cells were incubated with 5 μM DCFDA for 20 min at 37 °C at 7 days post-seeding. Nuclei were stained with Hoechst 3328 (Molecular Probes) to measure the total number of cells. Fluorescence intensity was measured by a fluorescent plate reader (Tecan) with 488 nm/515–545 nm (excitation/emission) for DCFDA, and 360 nm/460 nm (excitation/emission) for Hoechst. NO Fluorometric Assay Kit (BioVision) and TNF-α ELISA MAX Deluxe kit (BioLegend) were used to measure NO and TNF-α levels in the test culture media following the supplier's protocols. Background-subtracted values were normalized to the total number of cells for the measurement of intracellular H_2O_2 level and NO production, and to the total protein for the measurement of TNF-α secretion.

2.7. In vivo degradation of PEUR scaffolds implanted excisionally in rats

All surgical procedures were reviewed and approved by the Institutional Animal Care and Use Committee. Scaffolds were cut into 10 × 2 mm discs to measure the *in vivo* degradation rate. The discs were sterilized by gamma irradiation prior to implantation into dorsal excisional wounds (stented with stainless steel washers) in adult male Sprague–Dawley rats. Scaffolds were harvested at 7, 14, 21, and 28 days to evaluate the comparative rates of polymer degradation and new tissue formation within each of the scaffolds. The tissue was fixed in formalin for 24 h followed by incubation in 70% ethanol for 48 h, embedding in paraffin, sectioning, and staining with Gomori's trichrome and hematoxylin & eosin. Histomorphometric analysis of histological sections was performed to measure the scaffold degradation rates using Metamorph Imaging Software (Molecular Devices Inc, Sunnyvale CA).

Formalin-fixed paraffin-embedded tissues were sectioned at 5 μm, placed on slides, and warmed overnight at 60 °C. Slides were deparaffinized and rehydrated with graded alcohols ending in Tris buffered saline (TBS-T Wash Buffer, LabVision, Freemont, CA). Heat-mediated target retrieval was performed in 1X Target Retrieval Buffer (Citrate, pH 6.0, DAKO, Carpenteria, CA). Endogenous peroxidases and nonspecific background were blocked by subsequent incubations in 3% H_2O_2 in TBS-T and a serum mix consisting of 15% goat serum (Jackson ImmunoResearch, West Grove, PA), 5% rat serum (Invitrogen, Carlsbad, CA), and 1% BSA (Sigma, St. Louis, MO). Primary antibodies (Abcam, Cambridge, MA) to myeloperoxidase (1:200 for 30 min) or PGP9.5 were applied, followed by incubation in EnVision + HRP Labeled Polymer (RTU, DAKO). Slides were rinsed with TBS-T between each reagent applied treatment and all steps were carried out at room temperature. Visualization was achieved with DAB + chromogen (DAKO). Slides were counterstained with Mayer's hematoxylin, dehydrated through a series of alcohols and xylenes, and then coverslipped with Acrytol Mounting Media (Surgipath, Richmond, IL). Microscopic examination and imaging was performed with an Olympus BX60 microscope.

2.8. Statistical analysis

Statistical analysis of the results was performed using single factor analysis of variance (ANOVA). *P* values less than 0.05 were considered statistically significant.

3. Results

3.1. Effects of degradation time on mass loss and mechanical properties in vitro

During the first 8 weeks of *in vitro* incubation, all the PUR materials retained at least 80% of their original mass, but scaffolds synthesized from LTI degraded significantly faster than those prepared from HDIt at later time points (Fig. 1). The 6C/LTI material synthesized from the 6C polyester triol degraded more rapidly than the 7C/LTI material prepared from the 7C triol, a finding that is consistent with the previously reported half-lives of these polyesters (20 and 225 days, respectively [34]). The 6C/HDIt material with 50% PEG initially lost mass more rapidly than the 6C/HDIt scaffold without PEG, which may have resulted from greater swelling due to the hydrophilic PEG. However, the 6C/HDIt + 50% PEG material showed lower long-term mass loss, likely due to the higher content of non-hydrolysable polyether segments.

Compressive and tensile properties of the scaffolds were measured after 0, 4, 8, and 12 weeks of *in vitro* degradation. For all materials at all time points shown in Fig. 1B, scaffolds were compressed to 50% of their initial thickness without fracturing. Furthermore, the tensile strain at break ranged from 60 to 240% strain for all samples at all time points in Fig. 1C and D. These data show that the scaffolds maintained elastomeric mechanical properties and did not become brittle with time. For both compression and tensile testing, the Young's modulus, calculated from the initial linear slope of the stress–strain curves, decreased with time for all materials, which is consistent with the mass loss data (at 12 weeks, the 6C/LTI material could not be recovered in a form suitable for mechanical testing). While the tensile strength of the LTI scaffolds decreased significantly with time, the 6C/HDIt + PEG scaffold maintained relatively constant tensile strength for 12 weeks.

SEM images of the 7C/LTI scaffold at 0, 4, 8, and 12 weeks showed surface degradation, thinning, and pitting of the pore walls (Fig. 2). Surface erosion was evident at 4 and 8 weeks. At 12 weeks, the cumulative mass loss was ~10% (Fig. 1A), and pitting, cracking, and subsequent failure of pore walls was observed. Density and porosity measurements for all scaffolds at 0, 4, 8, and 12 weeks are listed in Table 2. For the HDIt scaffolds, the porosity did not change significantly for the first 12 weeks of degradation time. However, the porosity of the 7C/LTI scaffolds decreased after 12 weeks, and that of the 6C/LTI scaffolds decreased significantly at 8 weeks.

3.2. Effects of enzymatic and oxidative conditions on scaffold degradation in vitro

Scaffolds were incubated with the hydrolytic enzymes cholesterol esterase, carboxyl esterase, and lipase. These enzymes were chosen based on their previously reported effects on poly(ether-) and poly(carbonate-) urethane degradation, as they exhibited higher degradative activity than other esterases secreted from adherent macrophages [25,35]. Incubation with esterases slightly accelerated degradation relative to PBS, but few points were statistically significant ($p < 0.05$). Differences in degradation between the three candidate enzymes at any given time point were not significant. In contrast, incubation with

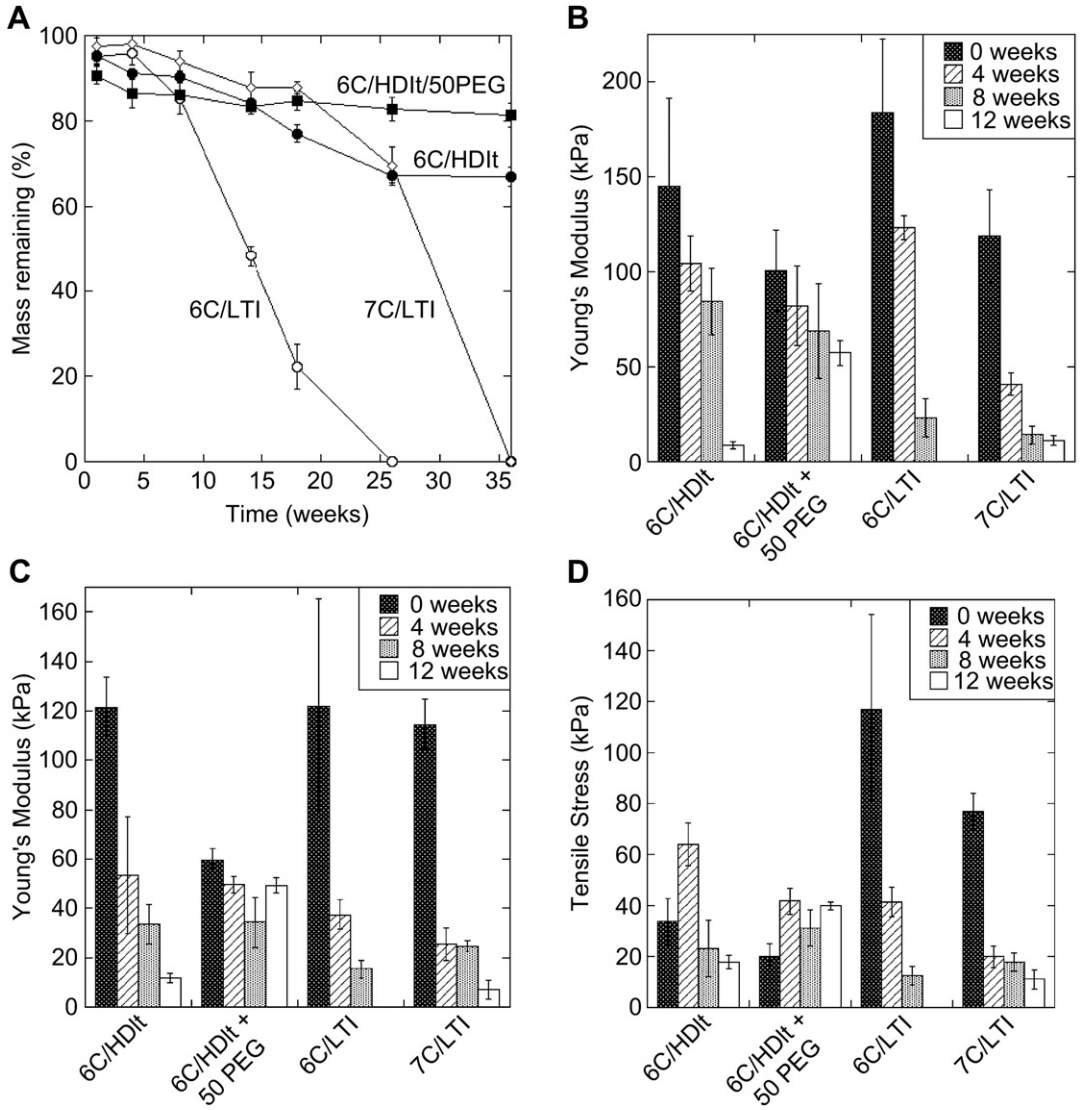

Fig. 1. Long-term *in vitro* degradation kinetics of LTI and HDIt scaffolds in PBS. LTI scaffolds undergo faster degradation, as measured by loss of mass and mechanical properties, compared to HDIt scaffolds. (A) Cumulative mass loss from 0 to 36 weeks. (B)–(D) Reduction in mechanical properties from 0 to 12 weeks. By 12 weeks LTI scaffolds had substantially degraded such that it was not possible perform the measurement. (B) Compressive modulus, (C) tensile modulus, and (D) tensile strength.

medium that created an oxidative microenvironment representative of the macrophage–material interface [29] had a more significant effect on the PUR degradation rate, especially for the LTI-based materials (Fig. 3D–F). The differences in mass loss between the buffer control and oxidative medium were statistically significant ($p < 0.05$) after 2 weeks for all materials except the 6C/HDIt + PEG, which interestingly degraded faster in the presence of cholesterol and carboxyl esterase than in oxidative medium. In Fig. 3F, data for each treatment group in oxidative medium are plotted to highlight differences between the LTI- and HDIt-based scaffolds. The 6C/LTI scaffold had completely dissolved by 4 weeks and the 7C/LTI scaffold by 6 weeks, while >50% of the mass of HDIt scaffolds remained at these time points.

3.3. Analysis of degradation products from PUR scaffolds

In vitro degradation of the scaffolds yielded water-soluble degradation products that under *in vivo* conditions would be anticipated to diffuse away from the defect site and be eliminated from the body. Structures of hypothesized degradation products and mechanisms are shown in Fig. 4. Hydrolysis of ester bonds was anticipated to yield α-hydroxy acids (e.g., hydroxycaproic, lactic, and glycolic acids), which was confirmed by HPLC (Fig. 5). The LTI scaffolds produced more α-hydroxy acids than HDIt scaffolds. The 7C/LTI formulation, which degraded more slowly due to the longer polyester half-life, yielded lower concentrations of α-hydroxy acids than the 6C/LTI formulation. Inclusion of PEG in the 6C/HDIt scaffold reduced the amount of α-hydroxy acids in the degradation medium due to the replacement of 50% of the polyester with PEG. Several unidentified peaks appeared in the HPLC spectra, which are conjectured to be adducts of α-hydroxy acids and either lysine or ethanolamine connected by urethane or urea bonds.

As shown in Fig. 4, oxidation of urethane and urea bonds was predicted to yield lysine and ethanolamine from LTI scaffolds, and cyanuric acid from HDIt scaffolds. Both lysine and ethanolamine were detected in the degradation products from LTI scaffolds when incubated in PBS; however, cyanuric acid was not detected in the degradation products from HDIt scaffolds. As shown in Fig. 6A, the amount of lysine recovered from 6C/LTI scaffolds was significantly

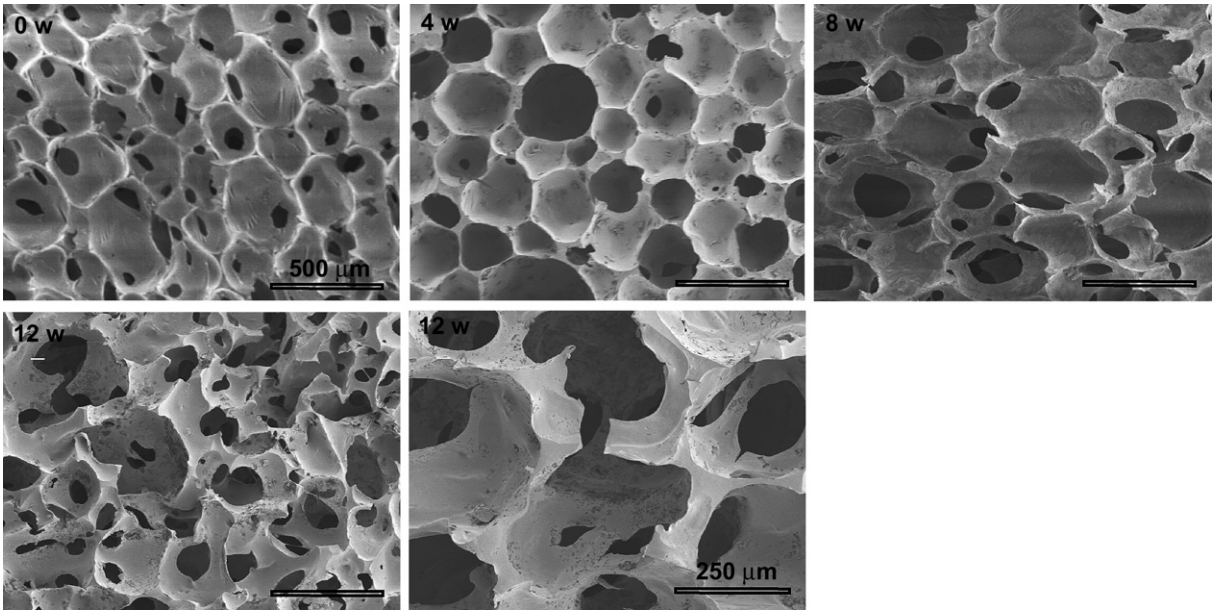

Fig. 2. Representative SEM images of 7C/LTI scaffolds after 0, 4, 8, and 12 weeks of *in vitro* degradation PBS. Surface erosion and pitting is evident as early as 4 weeks *in vitro*. Other scaffold formulations followed similar degradation patterns. Scale bar is 500 μm for the first four panels. In the final panel, a higher magnification view (scale bar 250 μm) shows thinning, cracking, and failure of pore walls at 12 weeks.

greater than that from 7C/LTI scaffolds after 14 weeks, which is consistent with the faster *in vitro* degradation of the 6C/LTI materials (Fig. 1). At 36 weeks, 18% of the lysine incorporated in the 6C/LTI scaffolds was recovered, while 100% of the original mass had degraded to soluble degradation products. This suggests that the majority of the lysine was incorporated in soluble urethane and urea adducts with α-hydroxy acids. The recovery of ethanolamine, which is released through hydrolysis of the ester group in LTI and a urethane bond, is shown in Fig. 6B. Ethanolamine was not detected (<0.001 μg/mg PUR) until 14 weeks, and at later time points the ethanolamine concentration increased with time. The recovery of ethanolamine upon complete dissolution of the 6C/LTI scaffold at 36 weeks was 9%.

3.4. *In vitro* culture of macrophages on PUR scaffolds

Murine monocyte-derived macrophages (RAW 264.7 cells) were cultured on the porous 6C/LTI scaffolds. After 2 weeks, SEM images (Fig. 7) of the fixed cells on the material surfaces revealed active individual macrophages (5–10 μm diameter, Fig. 7A–C) as well as groups of aggregated cells (20–30 μm, Fig. 7C). The material surface showed evidence of pitting (as large as 20 μm), similar to that observed for *in vitro* degradation in buffer without cells at later time points (e.g., 8–12 weeks *in vitro* incubation time). As shown in Fig. 7D, RAW 264.7 cells cultured on both 6C/LTI and 6C/HDIt scaffolds showed a significant increase in intracellular H_2O_2 relative to the tissue culture polystyrene control. Intracellular H_2O_2 measured for the 6C/HDIt group was also significantly higher than that measured for the 6C/LTI group. NO production (Fig. 7E) and TNF-α secretion (Fig. 7F) by cells cultured on both 6C/LTI and 6C/HDIt scaffolds were significantly lower than the control. Differences in NO production between the 6C/LTI and 6C/HDIt groups were significant.

Table 2
Bulk scaffold density (mg/cm^3) and porosity (vol-%) at various stages of degradation.

Material	Property	0 weeks	4 weeks	8 weeks	12 weeks
6C/HDIt	Density	98.2 ± 12.5	98.1 ± 6.0	101.0 ± 4.7	109.5 ± 7.1
	Porosity	*91.9 ± 1.0%*	*91.9 ± 0.5%*	*91.7 ± 0.4%*	*91.0 ± 0.6%*
6C/HDIt + 50 PEG	Density	93.7 ± 11.4	84.2 ± 4.6	90.7 ± 16.9	115.5 ± 5.5
	Porosity	*92.3 ± 1.0%*	*93.1 ± 0.4%*	*92.5 ± 1.4%*	*90.5 ± 0.5%*
6C/LTI	Density	87.5 ± 4.6	95.5 ± 6.2	198.7 ± 30.4	N/A
	Porosity	*92.8 ± 0.4%*	*92.1 ± 0.5%*	*83.5 ± 2.5%*	*N/A*
7C/LTI	Density	84.9 ± 14.0	65.9 ± 3.7	77.5 ± 0.6	183.5 ± 46.7
	Porosity	*93.0 ± 1.2%*	*94.6 ± 0.3%*	*93.6 ± 0.1%*	*84.8 ± 3.9%*

3.5. *Cell-mediated degradation of PEUR scaffolds in a rat excisional wound model*

In vivo degradation was determined by implanting 2 × 10 mm discs in excisional wounds in rats for up to 21 days. Early plasma permeation into the scaffold preceded cellular infiltration and formation of dense granulation tissue. Extracellular matrix with dense collagen fibers progressively replaced the characteristic, early cellular response. None of the implants engendered an overt inflammatory response or cytotoxicity, and fibroplasia and angiogenesis appeared to be equivalent among the different formulations.

As shown in Fig. 8A, LTI scaffolds degraded faster than the HDIt scaffolds, and at 28 days the differences in the amount of polymer remaining were significant. The *in vivo* rates of degradation of 6C/LTI and 7C/LTI scaffolds were consistent with the *in vitro* degradation rates in oxidative medium, which showed complete degradation after 4–6 weeks. However, after 8 weeks *in vitro*, the 6C/HDIt scaffolds were only 35% and 20% degraded in oxidative and esterolytic media, respectively, compared to ~60% degraded after 4 weeks *in vivo*. The incorporation of PEG into HDIt scaffolds slowed the degradation rate *in vivo*, while PEG accelerated the *in vitro* degradation rate (Fig. 1B). Each of the materials showed signs of fragmentation and breakdown mediated by a transient, giant cell, foreign body response *in vivo* (Fig. 8B and C). Anti-PGP9.5 staining of the histological sections highlighted the presence of macrophages and foreign body giant cells surrounding the material remnants, with fewer inflammatory cells in areas where new collagen and granulation tissue had formed after degradation of the PUR

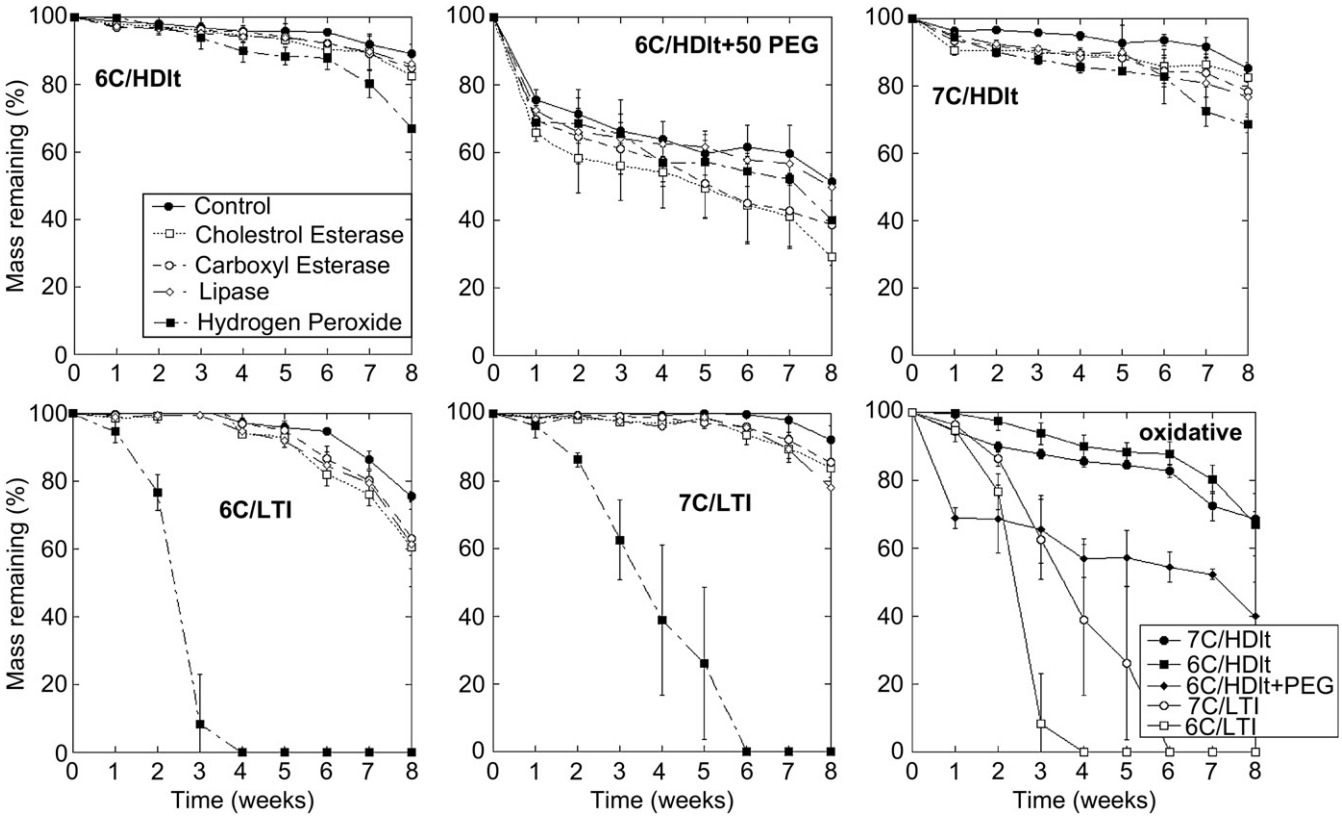

Fig. 3. Degradation of PUR scaffolds in enzymatic, oxidative, and control (PBS) media *in vitro*. Panels 1–5: Degradation profiles for 6C/HDIt, 6C/HDIt + 50 PEG, 7C/HDIt, 6C/LTI, and 7C/LTI scaffolds. Panel 6: Comparison of LTI and HDIt scaffolds in oxidative media showing the relatively faster degradation of LTI materials.

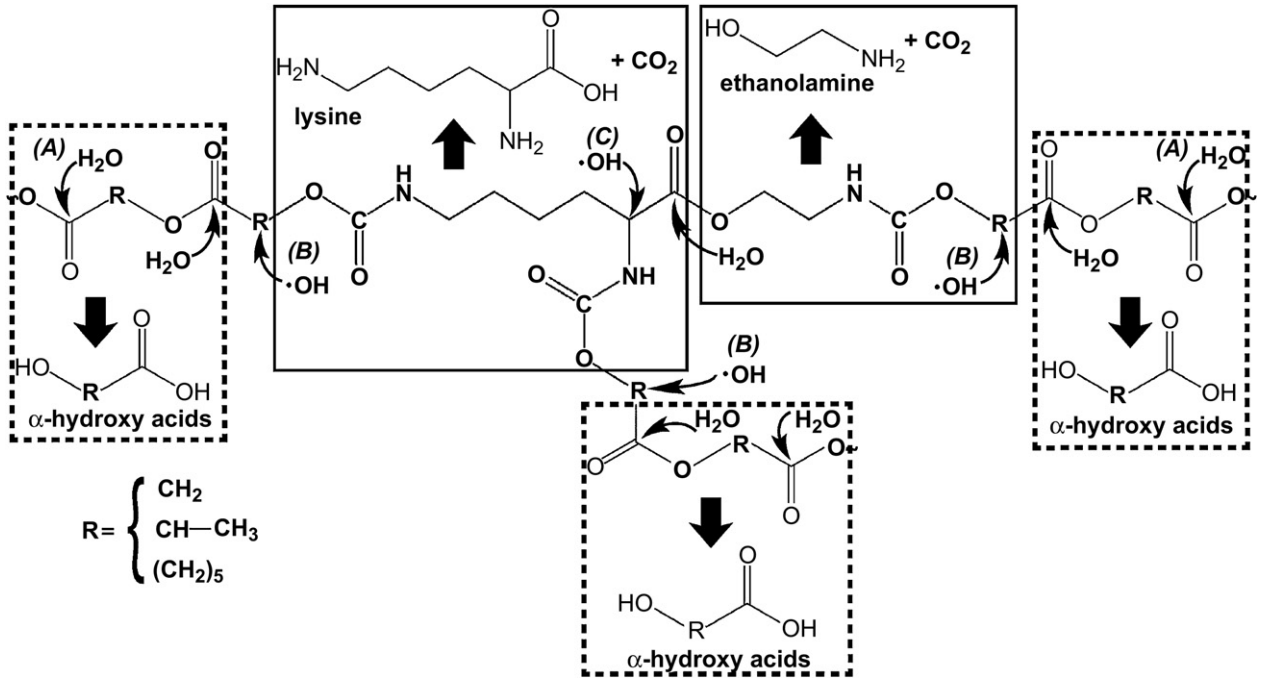

Fig. 4. Schematic showing hypothesized mechanisms of PUR scaffold degradation and soluble breakdown products. (A) Hydrolysis of ester bonds to yield α-hydroxy acids (dotted line). (B) Abstraction of the α-hydrogen atom in the R group adjacent to the urethane bonds by reaction with hydroxyl radicals to yield lysine or ethanoamine and carbon dioxide. (C) Abstraction of the α-hydrogen atom in lysine by reaction with hydroxyl radicals to yield multiple degradation products, including NH_4^+, α-ketoacids, oximes, CO_2, and carboxylic acids (degradation products not shown to simplify the diagram).

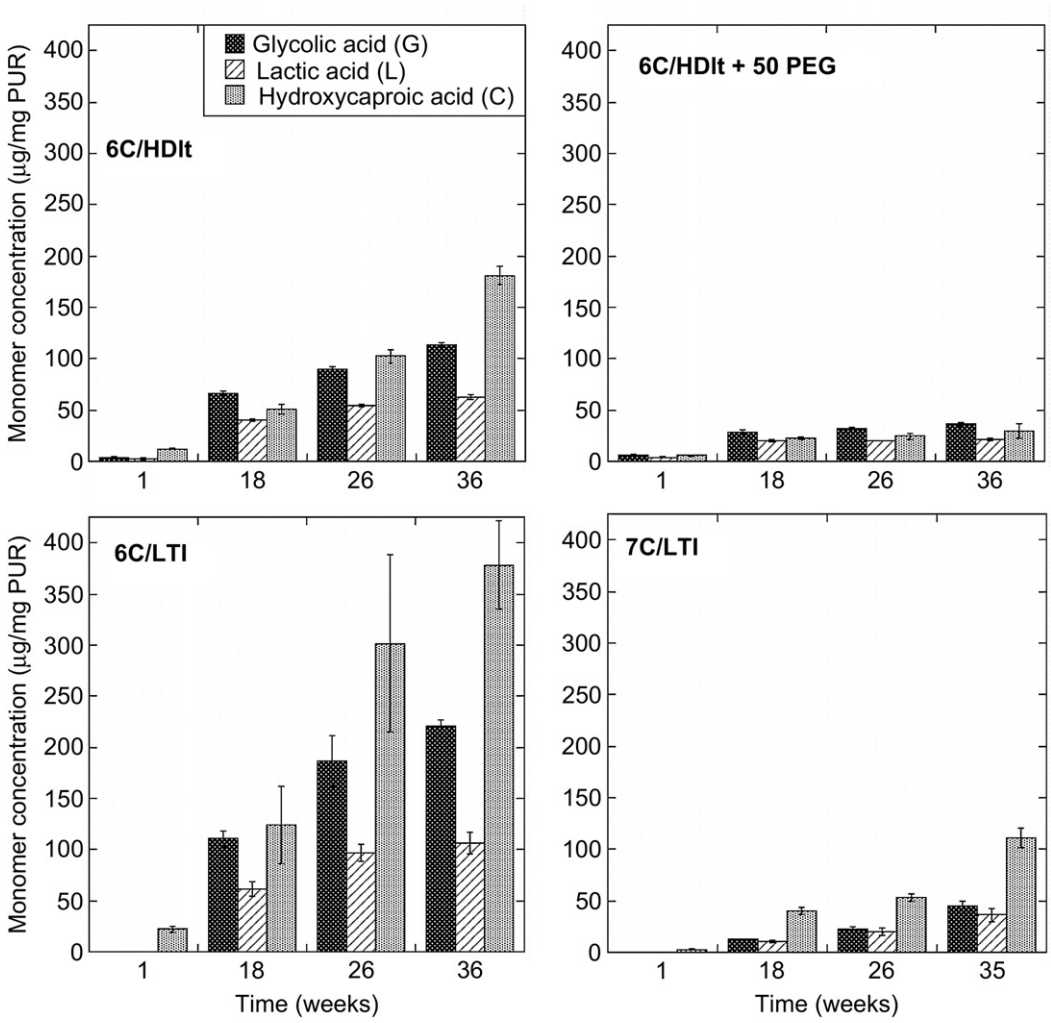

Fig. 5. Recovery of α-hydroxy acids from soluble degradation products of PUR scaffolds incubated in PBS for 36 weeks. (A) 6C/HDIt, (B) 6C/HDIt + 50 PEG, (C) 6C/LTI, and (D) 7C/LTI.

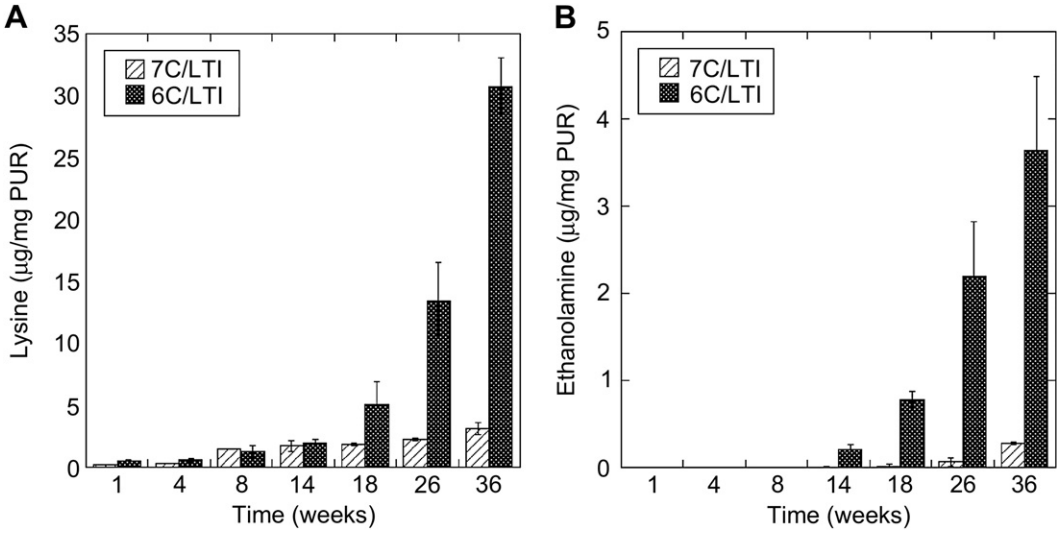

Fig. 6. Recovery of lysine and ethanolamine from the degradation medium measured by HPLC. Concentration of (A) lysine and (B) ethanolamine released from 6C/LTI and 7C/LTI scaffolds incubated in PBS for 36 weeks under cumulative release conditions.

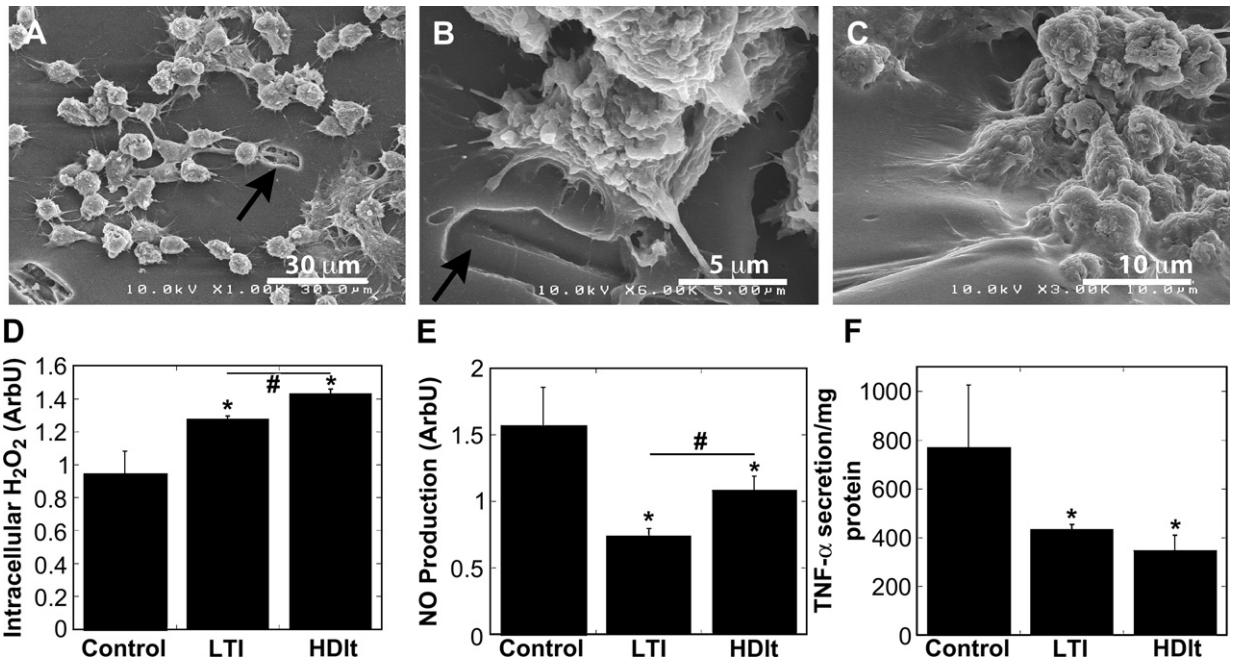

Fig. 7. SEM images of RAW 264.7 cells cultured on 6C/LTI scaffolds *in vitro* for 2 weeks. Low magnification (A) and high magnification (B) images show macrophage-mediated pitting and degradation of the scaffold. (C) Aggregation and early stage fusion of macrophages in the first step of giant cell formation. (D) Intracellular secretion of ROS by RAW 264.7 cells cultured on tissue culture polystyrene (control) and 6C/LTI and 6C/HDIt scaffolds at 7 days (arbitrary fluorescence units normalized by cell number). (E) NO production by RAW 264.7 cells at 7 days (arbitrary fluorescence units normalized by cell number). (F) Secreted TNF-α by RAW264.7 cells at 7 days (arbitrary units normalized by total protein).

remnants (Fig. 8D). Thus the images in Fig. 8B–D suggest that the inflammatory response was transient, as evidenced by the fewer numbers of macrophages far from the surface of the polymer remnants. Positive staining for myeloperoxidase (Fig. 8E and F) was consistent with localized production of ROS by the macrophages/giant cells surrounding material remnants. Taken together, the *in vivo* and *in vitro* data show that LTI scaffolds undergo macrophage-mediated degradation via hydrolytic and oxidative mechanisms.

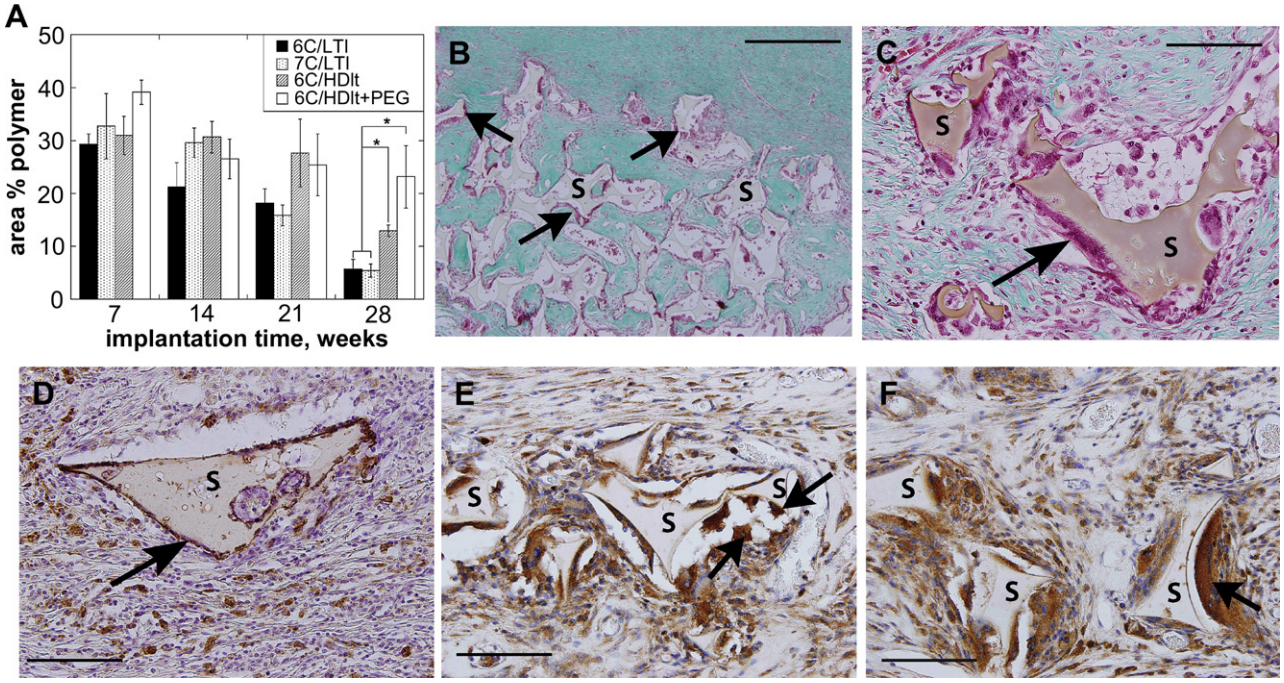

Fig. 8. (A) *In vivo* degradation rates measured by histomorphometry for 6C/LTI and 6C/HDIt scaffolds implanted sub-cutaneously in rats. (B, C) Presumed macrophages (magenta, indicated by arrows) line the edges of scaffold remnants as shown by trichrome staining of a 7C/LTI implant *in vivo* after 30 days. (D) Immunostaining (brown) for a macrophage marker (PGP9.5) verifies macrophage identity at the material surface and in nearby adjacent granulation tissue. Immunostaining for myeloperoxidase shows individual (E) and aggregated (F) macrophages expressing myeloperoxidase, the principal source of ROS. Scale bar = 200 μm (B), 75 μm (C) and 20 μm in C,E, F. scaffold = s.

4. Discussion

In this study, we investigated the hydrolytic, enzymatic, and oxidative degradation of LTI- and HDIt-derived PEUR scaffolds. Hydrolysis of ester bonds in the polyester triol yielded α-hydroxy acids (Fig. 5), which is consistent with previous studies [12,15,32,43,44]. The ester bond in LTI is also hydrolyzable to yield a carboxylic acid, which has been suggested to accelerate the degradation of lysine-derived polyurethanes through an autocatalytic mechanism [8], as well as increase the solubility of the breakdown products [45]. The cumulative recovery of lysine at complete degradation was 1.7% and 17% for the 7C/LTI and 6C/LTI materials, respectively, indicating that the majority of the lysine was incorporated in soluble adducts of α-hydroxy acids and triisocyanates, which have been shown to be non-cytotoxic *in vitro* [32,46]. In the long-term cumulative degradation experiments (Fig. 5), the medium was collected at each time point without periodic refreshing due to difficulties associated with handling the wet scaffolds at longer time points. While this approach minimized errors associated with solid–liquid phase separation [32], the concentration of lysine in the breakdown products was likely higher than under constant-sink conditions, where degradation products are removed at each sampling time point when the medium is refreshed. The extent of degradation of urethane and urea linkages in lysine-derived polyisocyanates is a topic of current debate, with some studies reporting up to 30% recovery of lysine [12,20] and others that these bonds can only be degraded enzymatically [11] due in part to the greater hydrolytic resistance associated with the semi-crystalline hard segment [26,36]. However, previous studies have shown that lysine-derived PEUR networks are microphase-mixed and lack semi-crystalline hard segments [32], suggesting that the urethane linkages are less tightly packed and thus more susceptible to hydrolytic and oxidative attack [26].

Ethanolamine was also released from LTI scaffolds by degradation of urethane and ester bonds, and the cumulative recovery was 9% at complete degradation. Ethanolamine oleate is used clinically as a sclerosing agent for the treatment of vascular lesions and cysts, and has been injected percutaneously at up to 15 g per injection (in a 5% EO solution) without significant side effects [47]. Furthermore, ethanolamine is the second most-abundant head group for phospholipids, and is phosphorylated by the enzyme ethanolamine kinase [48]. Thus considering the slow rate of release of ethanolamine, as well as its function in glycerophospholipid metabolism, its concentration is not anticipated to reach toxic levels *in vivo*.

After 4 weeks of incubation time, the mass loss of the scaffolds was <5% and the change in porosity insignificant, but the compressive modulus decreased by >60%. These observations are in agreement with a previous study reporting 30–50% losses in tensile strength at <10% mass loss for high porosity scaffolds fabricated from poly(ester urethane)urea elastomers [43]. The dramatic loss in mechanical properties is attributed to pitting and thinning of the pore walls and struts; for example, at 12 weeks the 7C/LTI scaffolds show ~10% mass loss (Fig. 1A) but extensive pitting of pore walls and cracking of struts (Fig. 2). These observations are in agreement with a previous study reporting pitting of poly(ether urethane)s after only ~10–15% soft segment mass loss [49]. Despite the loss in strength and modulus, the PEUR scaffolds maintained their elastomeric properties for at least 8–12 weeks. Over this time period, infiltration of cells and ingrowth of new tissue into the scaffold would be anticipated to increase the mechanical properties *in vivo*.

Macrophages accelerated the degradation of LTI and HDIt scaffolds *in vivo*, as evidenced by positive anti-PGP9.5 (Fig. 8D) and myeloperoxidase (Fig. 8E and F) staining of histological sections cut from 7C/LTI scaffolds. In some cases, macrophages fused into multinucleated foreign body giant cells (FBGCs, Fig. 8F), which occurs when macrophages encounter large particles (e.g., 10–100 μm) that cannot be phagocytosed [6,50], resulting in elevated cellular activation and secretion of degradative enzymes [6]. These observations are consistent with previous studies reporting macrophage-mediated enzymatic and oxidative degradation of biostable polyurethane implants [6,25,37,50–52]. An enclosed compartment forms at the macrophage–material interface, within which high local concentrations of ROS, acids, and enzymes are produced [40,49,53]. As shown in Fig. 7A–B, pitting of the pore walls at the macrophage–material interface was observed for RAW 264.7 cells cultured on 6C/LTI scaffolds.

Previous studies have shown that esterolytic enzymes secreted by macrophages degrade poly(ether-), poly(carbonate-), and poly (ester-) urethanes [26]. Cholesterol esterase has been reported to degrade both ester and urethane linkages, although the degradation of urethane bonds proceeds at a much lower rate [35]. Therefore, we investigated the effects of esterolytic enzymes on the *in vitro* degradation of LTI- and HDIt-derived PEUR networks. Incubation of scaffolds in cholesterol esterase, carboxyl esterase, and lipase modestly increased the rate of mass loss compared to buffer, but the differences were not significant until weeks 7 and 8. While previous studies have shown that cholesterol esterase more actively degrades PEURs than other enzymes [25], in the present study differences in degradation rates between the three candidate enzymes were insignificant for all materials (Fig. 3). Furthermore, the enzymatic degradation rates did not approach the *in vivo* rates, suggesting that esterolytic enzymes are not primarily responsible for degradation of PUR scaffolds *in vivo*.

In addition to esterolytic enzymes, macrophages also secrete ROS, which have been reported to mediate oxidative chain scission of poly(ether-) and poly(carbonate-) urethanes [29,36]. *In vitro* incubation of PUR scaffolds in oxidative media significantly accelerated PUR degradation with respect to the esterolytic enzymes and the buffer control (Fig. 3). The inclusion of PEG in the HDIt scaffolds increased the oxidative degradation rate compared to HDIt scaffolds without PEG (Fig. 3F), which is in agreement with previous studies reporting that polyethers undergo oxidative degradation [29]. LTI scaffolds degraded more than 6 times faster in oxidative media compared to the PBS control, and the rate of degradation in oxidative media *in vitro* approximated the *in vivo* rate. Considering that the degradation rates in pH 4 and pH 7 media were not significantly different, the faster degradation rate observed for the oxidative medium cannot be attributed to acid-catalyzed hydrolysis resulting from the low pH. To address the question whether LTI scaffolds activated macrophages, intracellular ROS, NO production, and TNF-α secretion were measured for RAW 264.7 cells cultured on 6C/LTI and 6CHDIt scaffolds and tissue culture polystyrene (control). Higher intracellular ROS levels in cells cultured on 6C/LTI and 6C/HDIt scaffolds relative to the control indicate that both scaffold types induced intracellular ROS production. The ROS level was significantly higher for 6C/HDIt compared to 6C/LTI scaffolds, and therefore the accelerated degradation of 6C/LTI scaffolds in oxidative medium cannot be attributed to increased activation of macrophages. In contrast, NO and TNF-α production were both lower for cells seeded on the PEUR scaffolds compared to the control. This observation is consistent with a previous report that TNF-α drives NO production [54]. Previous studies have shown that increased ROS production is indicative of the early stages of inflammatory cell activation [55], while NO is a key regulator of inflammatory cell deactivation and apoptosis [56]. Taken together, these results suggest that at 7 days inflammatory cells grown on the scaffolds were in the relatively early stages of activation, which might concomitantly delay the

induction of the late stage of inflammatory cell activation towards apoptosis, while cells in the control condition moved to the deactivation or the end stage of activation more rapidly.

To identify the mechanism of oxidative degradation of LTI scaffolds, we measured the concentrations of 6-hydroxycaproic and glycolic acids, ethanolamine, and cyanuric acid in the breakdown products. Lysine and lactic acid could not be measured by HPLC because the elution time of catalase added to reduce H_2O_2 overlapped with these components. The concentrations of ethanolamine (released from LTI scaffolds) and cyanuric acid (released from HDIt scaffolds) were <0.2 μg/ml at all time points in the oxidative medium (data not shown). In addition, the incremental recoveries of glycolic and 6-hydroxycaproic acids were $<1\%$ in both buffer and oxidative medium at both 2 and 6 weeks (data not shown). Thus the rates of ester and aliphatic urethane bond degradation in oxidative medium were comparable to those observed in buffer, which cannot account for the complete dissolution of LTI scaffolds in $\leq$6 weeks. Oxidation of the lysine residue may occur due to metal ion-catalyzed oxidation by H_2O_2, which proceeds by multiple pathways to yield NH_4^+, α-ketoacids, oximes, CO_2, and carboxylic acid degradation products [57]. As shown in Fig. 4C, these reactions are initiated by the abstraction of the α-hydrogen atom in lysine by reaction with hydroxyl radicals.

5. Conclusion

PEUR scaffolds prepared from HDIt and LTI undergo hydrolytic and macrophage-mediated degradation via esterolytic and oxidative mechanisms. In buffer, the primary mechanism of degradation was hydrolysis of ester bonds to yield α-hydroxy acids. Incubation of LTI and HDIt scaffolds in esterolytic media modestly increased the degradation rate. While HDIt scaffolds showed a modest ($<20\%$) increase in degradation rate in oxidative medium, LTI scaffolds degraded six times faster in oxidative medium. Furthermore, the *in vitro* rate of degradation of LTI scaffolds in oxidative medium approximated the *in vivo* rate in a rat excisional wound model. While recent preclinical studies have underscored the potential of injectable PEUR scaffolds and delivery systems for tissue regeneration [20,32,58], this promising class of biomaterials has a limited clinical history. Elucidation of the macrophage-mediated oxidative mechanism by which LTI scaffolds degrade *in vivo* provides key insights into the ultimate fate of these materials when injected into the body.

Acknowledgements

SEM images of RAW264.7 cells were captured through the use of the VUMC Cell Imaging Shared Resource. Funding was provided by the Department of Defense (Orthopaedic Extremity Trauma Research Program #W81XWH-07-1-0211), NIH grants AG06528 and AR056138, Vanderbilt Skin Diseases Research Core Center AR41493, and the Department of Veterans Affairs. The authors confirm that there are no known conflicts of interest associated with this publication and there has been no significant financial support for this work that could have influenced its outcome.

References

[1] Lewis D. Controlled release of bioactive agents from lactide/glycolide polymers. In: Chasin M, Langer R, editors. Biodegradable polymers as drug delivery systems. New York: Marcel Dekker, Inc.; 1990. p. 1–42.
[2] Rosen HB, Chang J, Wnek GE, Linhardt RJ, Langer R. Bioerodible polyanhydrides for controlled drug delivery. Biomaterials 1983;4(2):131–3.
[3] Pulapura S, Kohn J. Tyrosine-derived polycarbonates: backbone-modified "pseudo"-poly (amino acids) designed for biomedical applications. Biopolymers 1992;32(4):411–7.
[4] Laurencin CT, Koh HJ, Neenan TX, Allcock HR, Langer R. Controlled release using a new bioerodible polyphosphazene matrix system. J Biomed Mater Res 1987;21(10):1231–46.
[5] Yaszemski MJ, Payne RG, Hayes WC, Langer R, Mikos AG. In vitro degradation of a poly(propylene fumarate)-based composite material. Biomaterials 1996;17(22):2127–30.
[6] Anderson JM, Rodriguez A, Chang DT. Foreign body reaction to biomaterials. Sem Immunol 2008;20(2):86–100.
[7] Bruin P, Veenstra GJ, Nijenhuis AJ, Pennings AJ. Design and synthesis of biodegradable poly(ester-urethane) elastomer networks composed of non-toxic building blocks. Makromol Chem, Rapid Commun 1988;9:589–94.
[8] Storey RF, Wiggins JS, Puckett AD. Hydrolyzable poly(ester-urethane) networks from L-lysine diisocyanate and D, L-lactide/e-caprolactone homo- and copolyester triols. J Polym Sci Part A: Polym Chem 1994;32(12):2345–63.
[9] Saad B, Hirt TD, Welti M, Uhlschmid GK, Neuenschwander P, Suter UW. Development of degradable polyesterurethanes for medical applications: *in vitro* and *in vivo* evaluations. J Biomed Mater Res 1997;36:65–74.
[10] Borkenhagen M, Stoll RC, Neuenschwander P, Suter UW, Aebischer P. *In vivo* performance of a new biodegradable polyester urethane system used a nerve guidance channel. Biomaterials 1998;19:2155–65.
[11] Elliott SL, Fromstein JD, Santerre JP, Woodhouse KA. Identification of biodegradation products formed by L-phenylalanine based segmented polyurethaneureas. J Biomater Sci Polym Ed 2002;13(6):691–711.
[12] Zhang J-Y, Beckman EJ, Piesco NJ, Agarwal S. A new peptide-based urethane polymer: synthesis, biodegradation, and potential to support cell growth *in vitro*. Biomaterials 2000;21:1247–58.
[13] Zhang J-Y, Beckman EJ, Hu J, Yuang G-G, Agarwal S, Hollinger JO. Synthesis, biodegradability, and biocompatibility of lysine diisocyanate-glucose polymers. Tissue Eng 2002;8(5):771–85.
[14] Guelcher SA, Patel V, Gallagher K, Connolly S, Didier JE, Doctor J, et al. Synthesis and biocompatibility of polyurethane foam scaffolds from lysine diisocyanate and polyester polyols. Tissue Eng 2006;12(5):1247–59.
[15] Guelcher SA, Gallagher KM, Srinivasan A, McBride SB, Didier JE, Doctor JS, et al. Synthesis, in vitro biocompatibility and biodegradation, and mechanical properties of two-component polyurethane scaffolds: effects of water and polyol composition. Tissue Eng 2007;13(9):2321–33.
[16] Fujimoto KL, Tobita K, Merryman WD, Guan J, Momoi N, Stolz DB, et al. An elastic, biodegradable cardiac patch induces contractile smooth muscle and improves cardiac remodeling and function in subacute myocardial infarction. J Am Coll Cardiol 2007;49(23):2292–300.
[17] Li B, Davidson JM, Guelcher SA. The effect of the local delivery of platelet-derived growth factor from reactive two-component polyurethane scaffolds on the healing in rat skin excisional wounds. Biomaterials 2009;30(20):3486–94.
[18] Liljensten E, Gisselfaelt K, Nilsson A, Lindahl A, Edberg B, Bertilsson H, et al. Studies of poly(urethane urea) bands for ACL reconstruction. J Material Sci Mater Med 2002;13:351–9.
[19] Li B, Yoshii T, Hafeman AE, Nyman JS, Wenke JC, Guelcher SA. The effects of controlled release of BMP-2 from biodegradable polyurethane/microsphere composite scaffolds on new bone formation in rat femoral plug model. Biomaterials 2009;30(35):6768–79.
[20] Adhikari R, Gunatillake PA, Griffiths I, Tatai L, Wickramaratna M, Houshyar S, et al. Biodegradable injectable polyurethanes: synthesis and evaluation for orthopaedic applications. Biomaterials 2008;29(28):3762–70.
[21] Gogolewski S, Gorna K, Turner AS. Regeneration of bicortical defects in the iliac crest of estrogen-deficient sheep, using new biodegradable polyurethane bone graft substitutes. J Biomed Mater Res 2006;77A:802–10.
[22] Lelah MD, Cooper JL. Polyurethanes in medicine. Boca Raton, FL: CRC Press; 1987.
[23] Wang GB, Labow RS, Santerre JP. Biodegradation of a poly(ester)urea-urethane by cholesterol esterase: isolation and identification of principal biodegradation products. J Biomed Mater Res 1997;36(3):407–17.
[24] Tang YW, Labow RS, Santerre JP. Enzyme-induced biodegradation of polycarbonate polyurethanes: dependence on hard-segment concentration. J Biomed Mater Res 2001;56(4):516–28.
[25] Labow RS, Meek E, Matheson LA, Santerre JP. Human macrophage-mediated biodegradation of polyurethanes: assessment of candidate enzyme activities. Biomaterials 2002;23(19):3969–75.
[26] Santerre JP, Woodhouse K, Laroche G, Labow RS. Understanding the biodegradation of polyurethanes: from classical implants to tissue engineering materials. Biomaterials 2005;26(35):7457–70.
[27] McBane JE, Santerre JP, Labow RS. The interaction between hydrolytic and oxidative pathways in macrophage-mediated polyurethane degradation. J Biomed Mater Res A 2007;82A(4):984–94.
[28] Williams DF. Some observations on the role of cellular enzymes in polymer degradation. In: Syrett A, editor. Corrosion and degradation of implant materials: ASTM STP; 1979. p. 61–75.
[29] Christenson EM, Anderson JM, Hiltner A. Oxidative mechanisms of poly (carbonate urethane) and poly(ether urethane) biodegradation: *in vivo* and *in vitro* correlations. J Biomed Mater Res A 2004;70A(2):245–55.
[30] Zhao Q, Topham N, Anderson JM, Hiltner A, Lodoen G, Payet CR. Foreign-body giant cells and polyurethane biostability: *in vivo* correlation of cell adhesion and surface cracking. J Biomed Mater Res 1991;25(2):177–83.
[31] Guan J, Wagner WR. Synthesis, characterization, and cytocompatibility of polyurethaneurea elastomers with designed elastase sensitivity. Biomacromolecules 2005;6:2833–42.

[32] Hafeman AE, Li B, Yoshii T, Zienkiewicz K, Davidson JM, Guelcher SA. Injectable biodegradable polyurethane scaffolds with release of platelet-derived growth factor for tissue repair and regeneration. Pharm Res 2008;25(10):2387–99.
[33] Adhikari R, Gunatillake PA, inventors. Biodegradable polyurethane/urea compositions Patent No. WO 2004/009227 A2, 2004.
[34] Sawhney AS, Hubbell JA. Rapidly degraded terpolymers of D, L-lactide, glycolide, and ε-caprolactone with increased hydrophilicity by copolymerization with polyethers. J Biomed Mater Res 1990;24:1397–411.
[35] Labow RS, Meek E, Santerre JP. The biodegradation of poly(urethane)s by the esterolytic activity of serine proteases and oxidative enzyme systems. J Biomater Sci Polym Ed 1999;10(7):699–713.
[36] Schubert MA, Wiggins MJ, Anderson JM, Hiltner A. Role of oxygen in biodegradation of poly(etherurethane urea) elastomers. J Biomed Mater Res 1997;34(4):519–30.
[37] Labow RS, Meek E, Santerre JP. Model systems to assess the destructive potential of human neutrophils and monocyte-derived macrophages during the acute and chronic phases of inflammation. J Biomed Mater Res 2001;54(2):189–97.
[38] ASTM-International. D695–02a. Standard test method for compressive properties of Rigid Plastics; 2007.
[39] ASTM-International. D3574-05. Standard test methods for flexible cellular materials – slab, bonded, and molded urethane foams; 2007. pp. 360–368.
[40] Xia Z, Huang Y, Adamopoulos IE, Walpole A, Triffitt JT, Cui Z. Macrophage-mediated biodegradation of poly(D, L-lactide-co-glycolide) *in vitro*. J Biomed Mater Res A 2006;79A(3):582–90.
[41] Sung HJ, Yee A, Eskin SG, McIntire LV. Cyclic strain and motion control produce opposite oxidative responses in two human endothelial cell types. Am J Physiol Cell Physiol 2007;293(1):C87–94.
[42] Sung HJ, Chandra P, Treiser MD, Liu E, Iovine CP, Moghe PV, et al. Synthetic polymeric substrates as potent pro-oxidant versus anti-oxidant regulators of cytoskeletal remodeling and cell apoptosis. J Cell Physiol 2009;218(3):549–57.
[43] Guan J, Fujimoto KL, Sacks MS, Wagner WR. Preparation and characterization of highly porous, biodegradable polyurethane scaffolds for soft tissue applications. Biomaterials 2005;26:3961–71.
[44] Gorna K, Gogolewski S. Biodegradable porous polyurethane scaffolds for tissue repair and regeneration. J Biomed Mater Res Pt A 2006;79A (1):128–38.
[45] Tangpasuthadol V, Pendharkar SM, Kohn J. Hydrolytic degradation of tyrosine-derived polycarbonates, a class of new biomaterials. Part I: study of model compounds. Biomaterials 2000;21(23):2371–9.
[46] Guelcher SA, Srinivasan A, Dumas JE, Didier JE, McBride S, Hollinger JO. Synthesis, mechanical properties, biocompatibility, and biodegradation of polyurethane networks from lysine polyisocyanates. Biomaterials 2008;29:1762–75.
[47] Yamamoto K, Sakaguchi H, Anai H, Tanaka T, Morimoto K, Kichikawa K, et al. Sclerotherapy for simple cysts with use of ethanolamine oleate: preliminary experience. Cardiovasc Intervent Radiol 2005;28:751–5.
[48] Faulkner A, Turner JM. Phosphorylation of ethanolamine in catabolism: biodegradative adenosine triphosphate ethanolamine phosphotransferase and related enzymes in bacteria. Biochem Soc Trans 1974;2:133–6.
[49] Christenson EM, Patel S, Anderson JM, Hiltner A. Enzymatic degradation of poly(ether urethane) and poly(carbonate urethane) by cholesterol esterase. Biomaterials 2006;27(21):3920–6.
[50] Xia Z, Triffitt JT. A review on macrophage responses to biomaterials. Biomed Mater 2006;1(1):R1–9.
[51] Matheson LA, Labow RS, Santerre JP. Biodegradation of polycarbonate-based polyurethanes by the human monocyte-derived macrophage and U937 cell systems. J Biomed Mater Res 2002;61(4):505–13.
[52] Valentin JE, Stewart-Akers AM, Gilbert TW, Badylak SF. Macrophage participation in the degradation and remodeling of extracellular matrix scaffolds. Tissue Eng A 2009;15(7):1687–94.
[53] Heiple JM, Wright SD, Allen NS, Silverstein SC. Macrophages form circular zones of very close apposition to lgG-Coated surfaces. Cell Motil Cytoskeleton 1990;15(4):260–70.
[54] Jain B, Rubinstein I, Robbins RA, Sisson JH. TNF-alpha and IL-1 beta upregulate nitric oxide-dependent ciliary motility in bovine airway epithelium. Am J Physiol 1995;268:L911–7.
[55] Swindle EJ, Metcalfe DD. The role of reactive oxygen species and nitric oxide in mast cell-dependent inflammatory processes. Immunol Rev 2007;217: 186–205.
[56] Taylor EL, Megson IL, Haslett C, Rossi AG. Nitric oxide: a key regulator of myeloid inflammatory cell apoptosis. Cell Death Differ 2003;10:418–30.
[57] Stadtman ER. Oxidation of free amino acids and amino acid residues in proteins by radiolysis and by metal-catalyzed reactions. Annu Rev Biochem 1993;62(1):797–821.
[58] Dumas JE, Zienkiewicz K, Tanner SA, Prieto EM, Bhattacharyya S, Guelcher S. Synthesis and Characterization of an injectable allograft bone/polymer composite bone void filler with tunable mechanical properties. Tissue Eng Part A 2010;16(8):2505–18.